version of July 9, 2001

Submitted to

International Europhysics Conference on High Energy Physics, July 12, 2001, Budapest

EPS 2001:	Abstract:	**799**
	Parallel Session	**1**

XX International Symposium on Lepton and Photon Interactions, July 23, 2001, Rome

LP 2001:	Abstract:	**492**
	Plenary Session	**S7, S8**

www-h1.desy.de/h1/www/publications/conf/conf_list.html

A New Measurement of the Deep Inelastic Scattering Cross Section and of F_L at Low Q^2 and Bjorken x at HERA

H1 Collaboration

Abstract

Preliminary, new results are presented on the deep inelastic scattering cross section in the range of momentum transfers $Q^2 = 1.5 - 12$ GeV^2. The data were taken in 1999 by the H1 Collaboration at HERA, with positrons of 27.6 GeV energy and protons of 920 GeV energy, in a dedicated low Q^2 running period with an integrated luminosity of about 3 pb^{-1}. The cross section is measured to a few per cent accuracy with upgraded silicon tracking. It complements and extends a recent measurement of the proton structure functions $F_2(x, Q^2)$ and $F_L(x, Q^2)$ by H1 to even lower Bjorken x.

1 Introduction

The accurate measurement of the inclusive neutral current deep inelastic scattering (DIS) cross section $\sigma(ep \to eX)$ has been one of the prime tasks at HERA. The H1 Collaboration has recently published a comprehensive analysis [1] of data taken in the years 1996 and 1997 with beam energies $E_e = 27.6$ GeV and $E_p = 820$ GeV. The proton structure function $F_2(x, Q^2)$ was measured using the Born approximation of the reduced scattering cross section

$$\frac{Q^4 x}{2\pi\alpha^2 Y_+} \cdot \frac{d^2\sigma}{dx dQ^2} = \sigma_r = F_2(x, Q^2) - \frac{y^2}{Y_+} \cdot F_L(x, Q^2). \tag{1}$$

Here Q^2 is the four-momentum transfer squared carried by the virtual photon, y is the inelasticity and $x = Q^2/sy$ is the Bjorken variable. The beam energies determine the energy squared s in the centre of mass system, $s = 4E_e E_p$, and Y_+ is defined as $1 + (1 - y)^2$. The longitudinal structure function $F_L(x, Q^2)$ was accessed at large inelasticities y corresponding to the low x region.

The 1997 data for Q^2 below 15 GeV^2 were obtained in a dedicated running period with a luminosity of 1.8 pb^{-1}. In this range F_2 was measured to about 2-6% precision and F_L was determined with an absolute accuracy of about 0.15. In 1999 the H1 Collaboration has taken data at HERA with an increased proton beam energy E_p of 920 GeV in a further short running period with special triggers of 2.8 pb^{-1} luminosity. The purpose of this run was to complement the recent low Q^2 cross-section measurement and to obtain new data on the longitudinal structure function. The results are reported in this paper. The increased proton beam energy extends the phase space towards lower x at a given Q^2. An upgraded backward silicon tracker allows the range in y to be extended from 0.75 up to 0.89. The kinematic plane and its extension with the new 1999 data is illustrated in Figure 1.

This paper is organised as follows. Section 2 briefly describes the experimental methods, i.e. the kinematic reconstruction with the H1 detector, the event selection and simulation, calibration and background handling. The cross section measurement and the extractions of the structure functions are discussed in Section 3. A short summary is given in Section 4.

2 Experimental Methods

2.1 Kinematic Reconstruction with the H1 Detector

The event kinematics are reconstructed using the energy E'_e and the polar angle θ_e of the scattered positron according to the relations

$$Q_e^2 = \frac{E_e'^2 \sin^2 \theta_e}{1 - y_e} \qquad\qquad y_e = 1 - \frac{E'_e}{E_e} \sin^2(\theta_e/2) \tag{2}$$

which define the electron method of reconstruction. The scattered positron energy E'_e is measured in the backward electromagnetic lead-fibre calorimeter SPACAL [2]. The polar angle θ_e

is measured in the backward silicon tracker (BST). It is defined with respect to the proton beam direction, defining the z axis. The BST has an extended configuration of 8 concentric detector planes placed perpendicularly to the beam axis, each consisting of 16 wafers measuring the radial coordinate of tracks with an intrinsic resolution of better than 20 μm (r modules)[1]. A scattered positron candidate is defined as a vertex pointing track associated with the cluster in SPACAL of maximum energy having less than two Molière radii lateral extension.

Because of the degradation of the resolution of $y_e \propto 1/y$ the kinematics at low $y < 0.1$ are reconstructed using also information from the hadronic final state reconstructed in the Liquid Argon calorimeter (LAr) and the SPACAL, and from the central drift chambers, the jet chamber (CJC) and the z chambers [3]. This determines the inelasticity variable y to be

$$y_h = \frac{\sum_i (E_i - p_{z,i})}{2E_e} = \frac{\sum_h}{2E_e}, \tag{3}$$

where E_i and $p_{z,i}$ are the energy and longitudinal momentum component of a final state particle i, the masses being neglected. If a calorimeter cluster can be masked by a track in the central chambers, the momentum from the tracker is used instead of the LAr energy. In the analysis Q^2 and y are reconstructed using the Σ method which combines E_e, θ_e, and y_h according to

$$Q^2_\Sigma = \frac{E_e'^2 \sin^2\theta_e}{1 - y_\Sigma} \qquad\qquad y_\Sigma = \frac{y_h}{1 + y_h - y_e} = \frac{\sum_h}{\sum_h + E_e'(1 - cos\theta_e)}. \tag{4}$$

The hadronic scattering angle is defined as

$$\tan\frac{\theta_h}{2} = \frac{\sum_h}{P_{t,h}}, \tag{5}$$

where $P_{t,h}$ is the total transverse momentum of the hadronic final state particles.

The cross section is extracted using both the electron method and the sigma method. This allows important cross checks to be performed on the accuracy of the calorimeter calibrations and the final cross section to be obtained with optimum kinematic reconstruction.

The luminosity is determined from the cross section of the elastic bremsstrahlung process, measured with a precision of 1.2% . The luminosity measurement is by about 4% corrected for the occurence of proton beam satellites which do not enter the selected data sample.

2.2 Triggers and Event Selection

The data are triggered using the local energy sums in the SPACAL calorimeter with an energy threshold set to 5 GeV. This trigger is used in the main data analysis for the cross-section measurement for $y < 0.67$. In addition a high y trigger, accepting SPACAL energies down to 2 GeV, is realised by requiring a coincident vertex trigger signature in the proportional chamber

[1] In a pilot installation, made for one of the 16 ϕ sectors, the BST in 1999 was equipped with so-called ϕ detectors. These are wedge shaped, single sided Silicon detectors with strips parallel to one wafer edge at fixed ϕ. They are mounted back-to-back to the r detectors. Their efficiency is 98% based on a signal-to-noise ratio of 26.

z vertex position	$\lvert z\rvert < 30$cm
SPACAL cluster radius	< 4cm
SPACAL-BST matching	$\delta r < 2$cm
electromagnetic SPACAL energy	> 7 GeV
hadronic SPACAL energy	$< 15\%$ of E'_e
total $E - p_z$	> 35 GeV

Table 1: *Basic criteria to select DIS events. Note that in the high y data analysis, which extends down to 3 GeV, a second cluster in the SPACAL of energy larger than 2 GeV is required to reduce low energy background effects.*

system. These data are subject to a special, high y data analysis which is used for $0.89 > y > 0.67$.

Low energy deposits can also be caused by particles from events at very low $Q^2 \ll 1$ GeV^2 which mimic a positron signal in the Spacal. Part of these photoproduction background events is recognised by tagging a scattered positron in the electron tagger calorimeters upstream the positron beam.

The efficiency of all trigger elements exceeds 97% and is controlled by independent tracking triggers to an accuracy of 0.5%. From a monitor event sample, defined by a vertex accurately reconstructed in the central tracker and by a high energy SPACAL cluster ($E_e > 15$ GeV), the efficiency of all 128 BST r modules is determined to be 97% on average.

DIS events are required to have a vertex reconstructed from a track measured in the BST and its intersection with the beam axis. The track has to be associated with an electromagnetic energy deposition in the SPACAL (cluster) defined by a small lateral extension. Any energy behind the electromagnetic cluster measured in the hadronic SPACAL may not exceed a small fraction of E'. Radiative effects and background contributions are suppressed requiring energy-momentum conservation using the total $E - p_z$ reconstructed in the detector. All criteria are essential in distinguishing the genuine scattered positron from neutral or charged hadrons originating from photoproduction which otherwise by far exceeds the DIS signal at low energies. The criteria of the DIS event selection are summarised in Table 1.

A high statistics simulation of deep inelastic and photoproduction events is performed using the programs, GEANT [4], DJANGO [5] and PHOJET [6], and methods as described in [1]. Simulated events are subject to the same reconstruction and analysis chain as the real data. In the comparisons of experimental distributions with the Monte Carlo spectra, these are normalised to the measured luminosity.

2.3 Alignment and Calibration

The measurement of θ_e requires the BST to be accurately aligned. After the internal adjustment of the detector planes, the BST is aligned using the z position of the interaction vertex z_v. This is determined by the central tracker which defines the H1 coordinate system and measures the inclination of the beam with respect to the detector axis. A measurement accuracy of θ_e of 0.2 mrad is obtained by comparing the angle measured in the BST with the one resulting from

z_v and the hit position in the backward drift chamber (BDC). The alignment of the ϕ detectors is done using the vertex position and approximating tracks in the strip coordinates by a quadratic form. From high energy tracks, a resolution of better than 20μm is measured and the modules are found to be aligned to within 5μm accuracy. The SPACAL position is adjusted using QED Compton events which have the signature of back-to-back positron and photon clusters.

The energy scale of the electromagnetic SPACAL cells in the region of large $E' > 17$ GeV is determined from the measurement of the angles θ_e and θ_h to within a remaining uncertainty of 0.3%. This scale is verified in the low energy range to better than 2% from a comparison of E' with the corresponding momentum p, measured with the BST, and the transverse vertex position, see Section 2.4. The hadronic energy scales in the LAr calorimeter and in the SPACAL are determined to an accuracy of 2% and 5%, respectively, using a global minimisation technique [7] for the influence of the calorimeter constants on the transverse momentum balance for the DIS events. A direct verification of the electromagnetic and the hadronic energy scale uncertainty is obtained from an extension of the cross section measurement, using the electron method to very low $y \geq 0.005$ and the sigma method to large $y \leq 0.6$, respectively. The resulting cross sections agree to within the statistical accuracy.

2.4 Estimation of Photoproduction Background

The present analysis includes data down to $E' = 3$ GeV which is the smallest scattered positron energy reached so far in the low Q^2 inclusive cross section measurements of H1 [1]. In this range the photoproduction background is large. For most of the DIS events a second particle, besides the positron, is scattered into the backward region. Thus for the data at $y > 0.67$ two clusters in the SPACAL are required for a DIS candidate event. This requirement reduces the photoproduction background by a factor of about 5 while retaining 90% of the genuine DIS events as estimated in the simulation.

The remaining photoproduction background is subtracted using a high statistics PHOJET simulation which is normalised using the photoproduction events registered in the electron tagger. This normalisation is verified by a complementary analysis to within 25% utilising the track momentum measurement with the BST. This enables, on a statistical basis, the photoproduction background to be removed from the DIS positron signal, see Section 3.1.

Figure 2 shows the distribution of the ratio of the energy E measured in the SPACAL to the momentum p measured with the BST $r - \phi$ detectors in two intervals of E. For low energies a small enhancement is observed at about $E/p \simeq -1$. This represents the negatively charged background[2] to the truely DIS signal which dominates the peak at $E/p \simeq +1$. At larger energies, the background is seen to be reduced to a much smaller level. The peak position for positive charges represents a verification of the SPACAL low energy scale at the per cent level of accuracy.

[2]From the tagged events a charge asymmetry of $6 \pm 3\%$ is determined, in agreement with [1], which is corrected for in the dedicated $r - \phi$ BST analysis.

3 The Cross Section and the Proton Structure Functions

3.1 Data and Simulation Comparisons

A precise measurement of the DIS cross section requires the data to be corrected for acceptance, inefficiency, resolution and radiative effects. It is thus important to compare experimental and simulated distributions. Such control distributions related to the main data analysis are for $E' > 7$ GeV shown in Figure 3. The experimental distributions for the basic kinematic variables, the scattered positron energy E' and angle θ_e and the inelasticity y_h are seen to be well described by the DIS simulation. The event selection criteria, discussed in Section 2.2, reduce the photoproduction background in this analysis and energy range to a very small level.

Control distributions for the high y region are displayed in Figures 4 and 5. The Q^2_e and y_e distributions in Figure 4 are seen to be well described by the simulation of DIS and photoproduction events. The normalisation of the simulated photoproduction background is based on the tagged event sample and, as explained in Section 2.4, it is verified with a special data analysis utilising the BST momentum measurement. Figure 5 shows the scattered energy and angle distributions in this dedicated analysis. The background shown is determined from data with a track of negative charge. The histogram represents the sum of this experimentally measured background and of the simulation of the genuine DIS events. The understanding of the data down to 3 GeV scattered positron energy allows the measurement of cross sections at high y which are essential for the F_L determination.

3.2 Systematic Uncertainties

The uncertainties of this cross section measurement are divided into four different kinds:

- The data have a normalisation uncertainty of 1.3% resulting from the uncertainty of the luminosity measurement (1.2%) and of the trigger efficiency determination (0.5%). This uncertainty is not included in any error bar subsequently shown.
- The statistical uncertainty of the data is about 2%.
- An about 2% uncorrelated cross-section uncertainty is due to the Monte Carlo event statistics. Moreover, uncorrelated errors with weak kinematic dependencies result from the BST track reconstruction (1-2%), from the uncertainty of the radiative corrections (0.5%) and from the positron identification uncertainty (1%).
- Correlated cross-section uncertainties result from the E' and E_h measurements (0.5-2%), from the θ_e reconstruction (0.5%), the calorimeter noise (2% at low y) and from the photoproduction background (5% at high y).

The total cross-section uncertainty is about 3% in the bulk data region increasing to about 7% at the edges of the y range covered. This is comparable to the low Q^2 data recently published by the H1 Collaboration [1].

3.3 Determination of the Cross-Section and Extraction of $F_2(x, Q^2)$

The kinematic region accessed in this measurement is divided into eight Q^2 intervals for a range $1 < Q^2 < 14$ GeV^2, as used previously. Since an essential goal of this analysis has been the extraction of F_L, the x range is subdivided using the $y = Q^2/sx$ variable. At high y, bin edges ($y = 0.89,\ 0.79,\ 0.67,\ 0.53$) are chosen which are adapted to the y bins used for the 820 GeV data analysis [3]. Below this range four y intervals per decade are used until at $y \leq 0.016$ the bin size is doubled. The binning is well adapted to the resolution in the measurement of the kinematic variables. Bins are accepted if the purity and stability are bigger than 30% with typical values being 70%. Here the purity (stability) is defined as the number of simulated events which originate from a bin and which are reconstructed in it, divided by the number of reconstructed (generated) events in that bin.

The measured reduced cross section [8, 9] (Equation 1) is shown in Figure 6. The cross section rises towards low x until it is tamed and σ_r even turns over at x values corresponding to $x \simeq Q^2/0.6s$. This behaviour, for $Q^2 \geq 2.5$ GeV^2, is well described by the NLO QCD fit to the 820 GeV data which is discussed in detail in [1]. Note that this fit used H1 data with a minimum Q^2 of 3.5 GeV^2. The extrapolation to lower $Q^2 < Q^2_{min}$ is again found to be lower than the measured data, in particular at high y.

Using the NLO QCD calculation of F_L, the proton structure function $F_2(x, Q^2)$ is extracted from the data. The analysis has been limited to maximum y values of 0.6 in order to reduce the effect of the calculated F_L on F_2 to the few per cent level. It is seen in Figure 7 that the new data agree well with the recently published H1 data and also with the data from the NMC Collaboration [10] obtained in deep inelastic, fixed-target muon-proton scattering. The rise of F_2 towards low x is observed to be continuous beyond the previously accessible kinematic range extending the observation recently made [11]. At larger x the data extend into the kinematic region of the fixed target experiments, and good agreement is found.

3.4 The Longitudinal Structure Function $F_L(x, Q^2)$

The measured cross section is sensitive to the longitudinal structure function $F_L(x, Q^2)$ at low x. An extension towards lower x than accessed in [1] is achieved with the increase of the proton beam energy, from 820 GeV to 920 GeV, and of the maximum y, from 0.75 to 0.89.

A suitable method, introduced in [1], to extract F_L at low Q^2 is based on the partial derivative of the reduced cross section, taken at fixed Q^2, i.e.

$$\left(\frac{\partial \sigma_r}{\partial \ln y}\right)_{Q^2} = \left(\frac{\partial F_2}{\partial \ln y}\right)_{Q^2} - F_L \cdot 2y^2 \cdot \frac{2-y}{Y_+^2} - \frac{\partial F_L}{\partial \ln y} \cdot \frac{y^2}{Y_+}. \qquad (6)$$

Contrary to the cross section itself, the F_L contribution to this derivative is of size similar to the F_2 contribution. Taking into account the systematic error correlations, the derivative is determined for a rebinned Q^2 division of the data. The derivative is shown in Figure 8 and, for illustration, compared with the NLO QCD fit result using different assumptions on F_L.

[3] The previous analysis extended to a maximum y of 0.75 which corresponds to $y = 0.67$ for $E_p = 920$ GeV.

For $y \leq 0.2$, straight line fits are performed in $\ln y$ to the derivative $(\partial \sigma_r / \partial \ln y)_{Q^2}$. These are extrapolated to determine the contribution of $(\partial F_2 / \partial \ln y)_{Q^2}$ at high y and to subtract it from the cross section derivative. The uncertainty on this extrapolation is included in the systematic errors of F_L , taking into account the correlations of errors at low y with those at high y. The contribution of the F_L derivative is calculated to be negligible using parton distribution parameterisations and also the H1 QCD fit. The estimated size is added to the systematic uncertainty of the F_L extraction.

The new data points for $F_L(x, Q^2)$ are shown in Figure 9. They extend into a lower range of x and are consistent with the previous H1 result. The curves are a NLO QCD calculation of F_L based on a fit to the previous F_2 data for $y < 0.35$, i.e. in a region where F_2 is practically independent of F_L . An overview of the full H1 data, obtained for $F_L(x, Q^2)$ from $Q^2 = 2.2$ GeV^2 to 700 GeV^2 [12], is given in Figure 10. The apparent rise of $F_L(x, Q^2)$ towards low x is related to a large gluon momentum distribution. At the presently reached accuracy, all data are well described by the NLO QCD calculation in which the gluon distribution is determined from the scaling violations of $F_2(x, Q^2)$.

4 Summary

A new measurement of the deep-inelastic positron-proton scattering cross section is presented for squared four-momentum transfers $1.5 \leq Q^2 \leq 12\ \mathrm{GeV}^2$ and Bjorken-x values $2 \cdot 10^{-5} \leq x \leq 0.07$. These data are complementary to low Q^2 data recently published as they are taken at a proton beam energy increased to 920 GeV and measured with an upgraded backward silicon tracker. The new ability to measure low particle momenta with the BST allows the analysis to be reliably performed down to 3 GeV of scattered positron energy. The kinematic range is thus extended towards lower x and larger $y \leq 0.89$, respectively.

The accuracy of these cross section data is about 3% in most of the kinematic range. The cross section is well described by a NLO QCD analysis performed on previous H1 cross-section data. It exhibits a turn over at low x, for fixed large $y \simeq 0.6$, which is thus attributable to the influence of the longitudinal structure function.

The new $F_2(x, Q^2)$ data confirm and complement the H1 data recently published. The rise of F_2 towards low x is observed to continue beyond the previously accessible kinematic range. At larger x the data extend into the kinematic region of the fixed target muon-proton scattering experiments, and good agreement is found.

The partial derivative of the reduced cross section, $(\partial \sigma_r / \partial \ln y)_{Q^2}$, is measured and used to obtain new data on the longitudinal structure function $F_L(x, Q^2)$. The data extend to lower x and are, in the region of overlap, consistent with previous determinations of F_L .

Acknowledgements We are very grateful to the HERA machine group whose outstanding efforts made this experiment possible. We acknowledge the support of the DESY technical staff. We appreciate the substantial effort of the engineers and technicians who constructed and maintain the detector. We thank the funding agencies for financial support of this experiment. We wish to thank the DESY directorate for the support and hospitality extended to the non-DESY members of the collaboration.

References

[1] C. Adloff *et al.* [H1 Collaboration], DESY-00-181, Eur. Phys. J. C, to appear, [hep-ex/0012153].

[2] R. Appuhn *et al.*, Nucl. Instr. and Meth. **A386** (1996) 397.

[3] I. Abt *et al.* [H1 Collaboration], Nucl. Instr. and Meth. **A386** (1997) 310 and **A386** (1997) 348.

[4] R. Brun *et al.*, GEANT3 User's Guide, CERN-DD/EE 84-1, Geneva (1987).

[5] G. A. Schuler and H. Spiesberger, Proc. Workshop on HERA Physics, Vol 3, eds. W. Buchmüller and G. Ingelman, Hamburg, DESY (1992), p. 1419;
A. Kwiatkowski, H. Spiesberger and H.-J. Möhring, Comp. Phys. Comm. **69** (1992) 155;
L. Lönnblad, Comp. Phys. Comm. **71** (1992) 15.

[6] R. Engel and J. Ranft, Phys. Rev. **D54** (1996) 4244.

[7] V.V. Arkadov, PhD Thesis, Berlin, Humboldt-University, 2000, DESY-Thesis-2000-046.

[8] D. Eckstein, PhD Thesis, Berlin, Humboldt-University, in preparation.

[9] T. Laštovička, PhD Thesis, Berlin, Humboldt-University, in preparation.

[10] M. Arneodo *et al.* [NMC Collaboration], Nucl. Phys. **B483** (1997) 3.

[11] C. Adloff *et al.* [H1 Collaboration], *A Measurement of the Rise of $F_2(x, Q^2)$ towards Low x*, paper 141, submitted to the EPS Conference, Budapest, 2001.

[12] C. Adloff *et al.* [H1 Collaboration], *Measurement of Neutral and Charged Current Cross Sections and of F_L at High Q^2*, paper 803, submitted to the EPS Conference, Budapest, 2001.

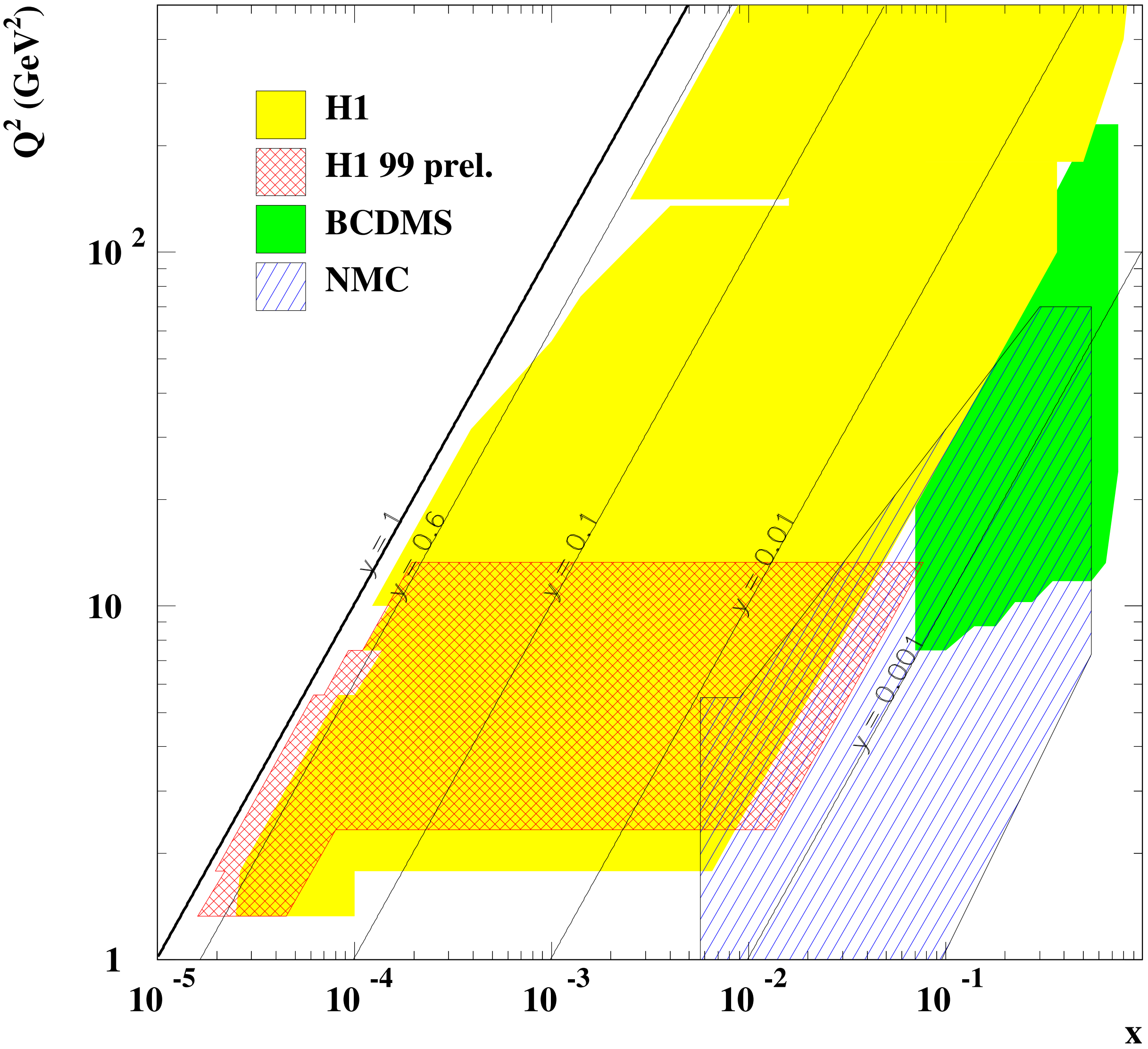

Figure 1: Kinematic region covered by this measurement at 920 GeV proton beam energy, by the recently published H1 data at 820 GeV and by the muon-proton scattering experiments NMC and BCDMS. The lines of constant y correspond to this analysis, i.e. $E_e = 27.6$ GeV and $E_p = 920$ GeV.

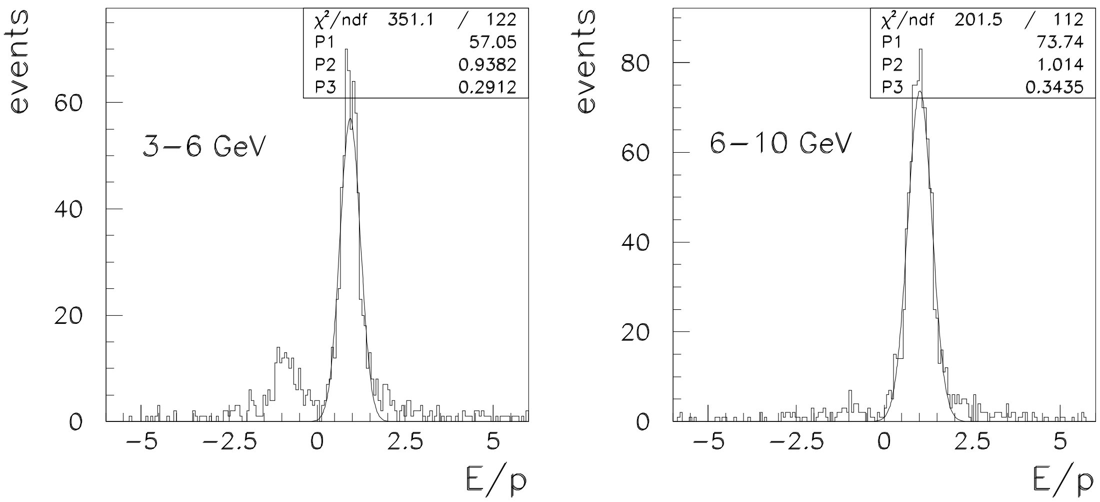

Figure 2: Ratio of the energy measured in the SPACAL calorimeter and the momentum measured with the BST r- and ϕ-detectors for two energy ranges. The enhancement at about -1 is due to negatively charged tracks mainly due from photoproduction events. The peak at $+1$ is due to scattered positrons with a small admixture of background. Events are selected according to the requirements quoted in Table 1.

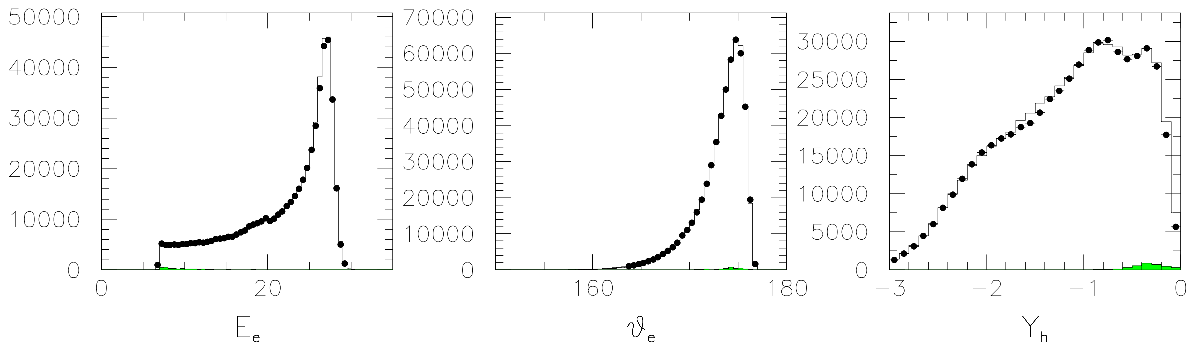

Figure 3: Event distributions of the energy and the polar angle of the scattered positron candidates, and of y_h in the main data analysis. The histograms represent the simulation of DIS and the small photoproduction background (shaded).

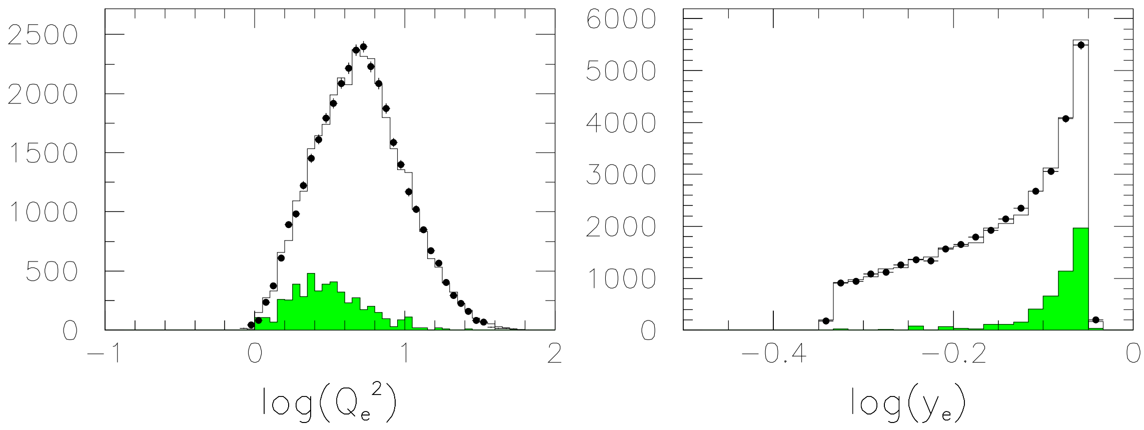

Figure 4: Even distributions of Q^2 and y of the scattered positron candidates, illustrating the cross section measurement at high y. Solid points: H1 data; shaded histograms: simulation of photoproduction events; open histograms: added distributions of simulated DIS and photoproduction events.

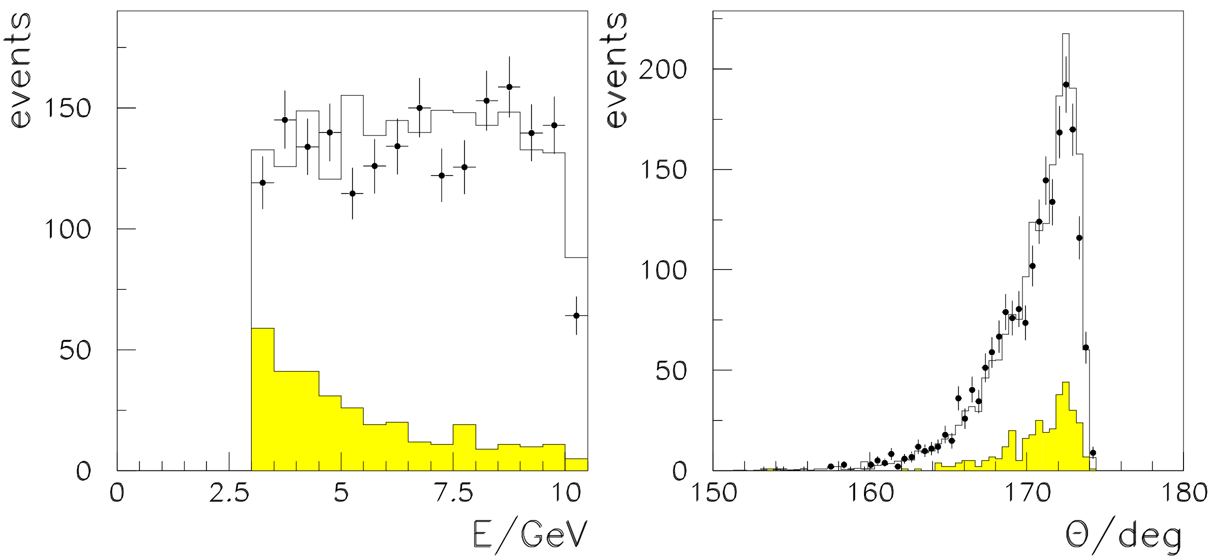

Figure 5: Distributions of the energy and polar angle θ_e of the scattered positron in a high y data analysis employing the charge measurement with the BST r and ϕ detectors in 1/16 of 2π. Solid points: data with positive charge assignment; open histogram: sum of data with negative charge assignment and DIS event simulation, normalised to the data luminosity. The distributions are shown before subtracting the measured background (shaded histogram) given by data with negative charge assignment.

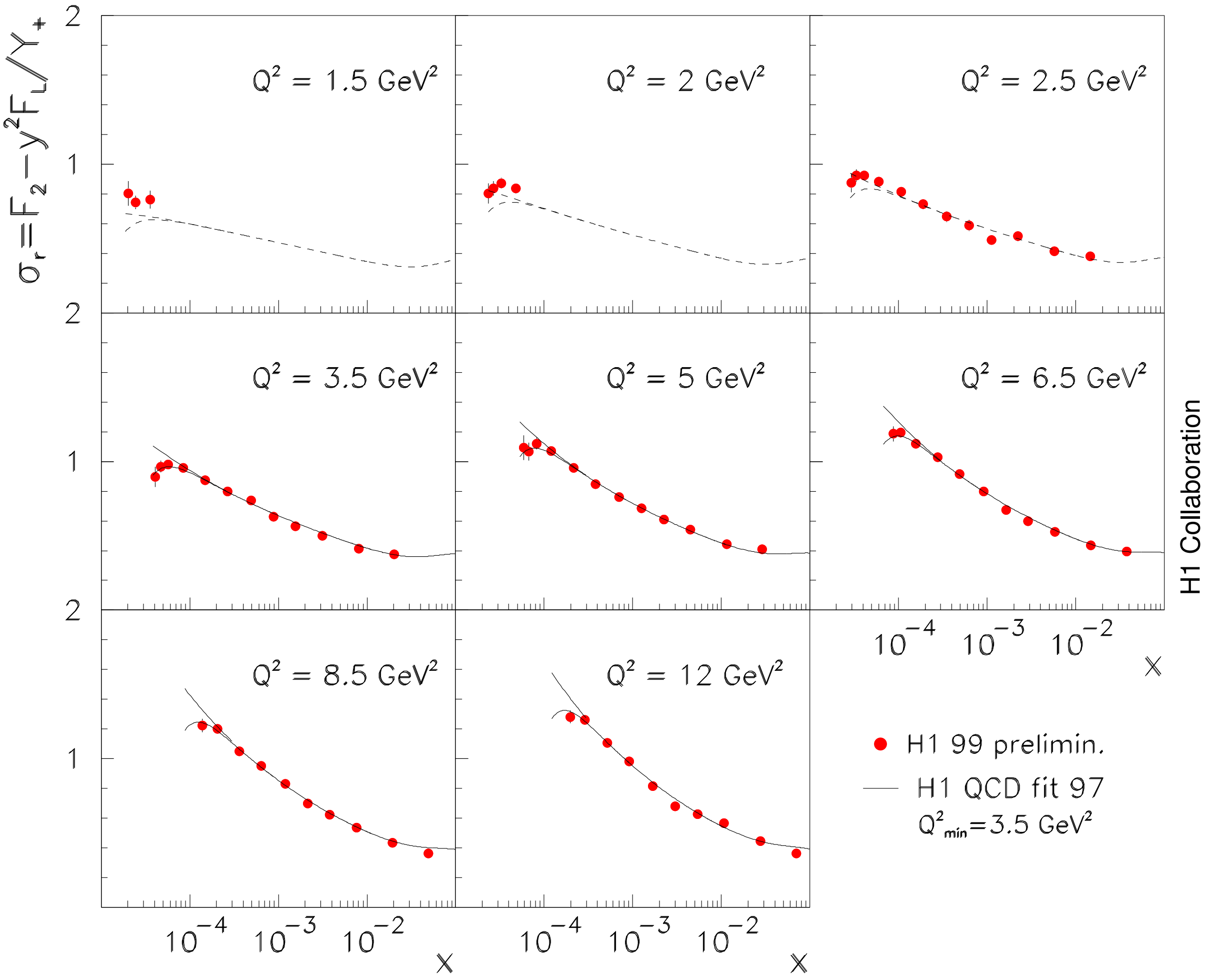

Figure 6: Measurement of the reduced DIS cross section (closed points) from the 920 GeV proton energy data taken in 1999. The curves represent a NLO QCD fit to the H1 1996/97 data which was limited to $Q^2 \geq 3.5$ GeV^2. The dashed curves show the extrapolation of this fit below Q^2_{min}. For each Q^2 bin two curves are drawn which represent the reduced cross section σ_r (lower curve, turning at low x) and the structure function F_2, which rises towards low x (upper curve). For larger x, corresponding to lower y, $\sigma_r \simeq F_2$.

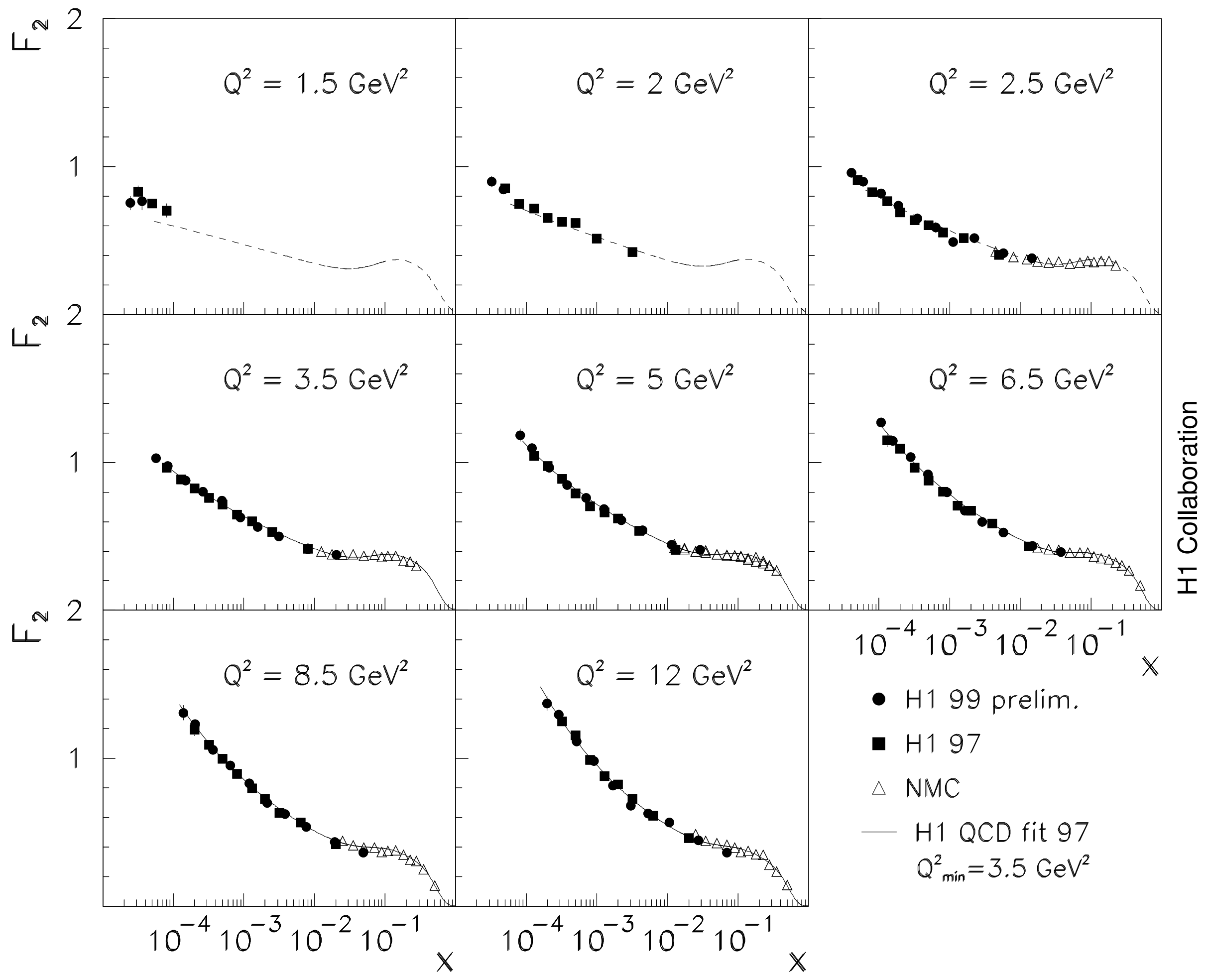

Figure 7: Measurement of the structure function $F_2(x, Q^2)$ by the H1 and NMC experiments. The curves represent a NLO QCD fit to the H1 96/97 data which was limited to $Q^2 \geq 3.5$ GeV^2. The dashed curves show the extrapolation of this fit below Q^2_{min}.

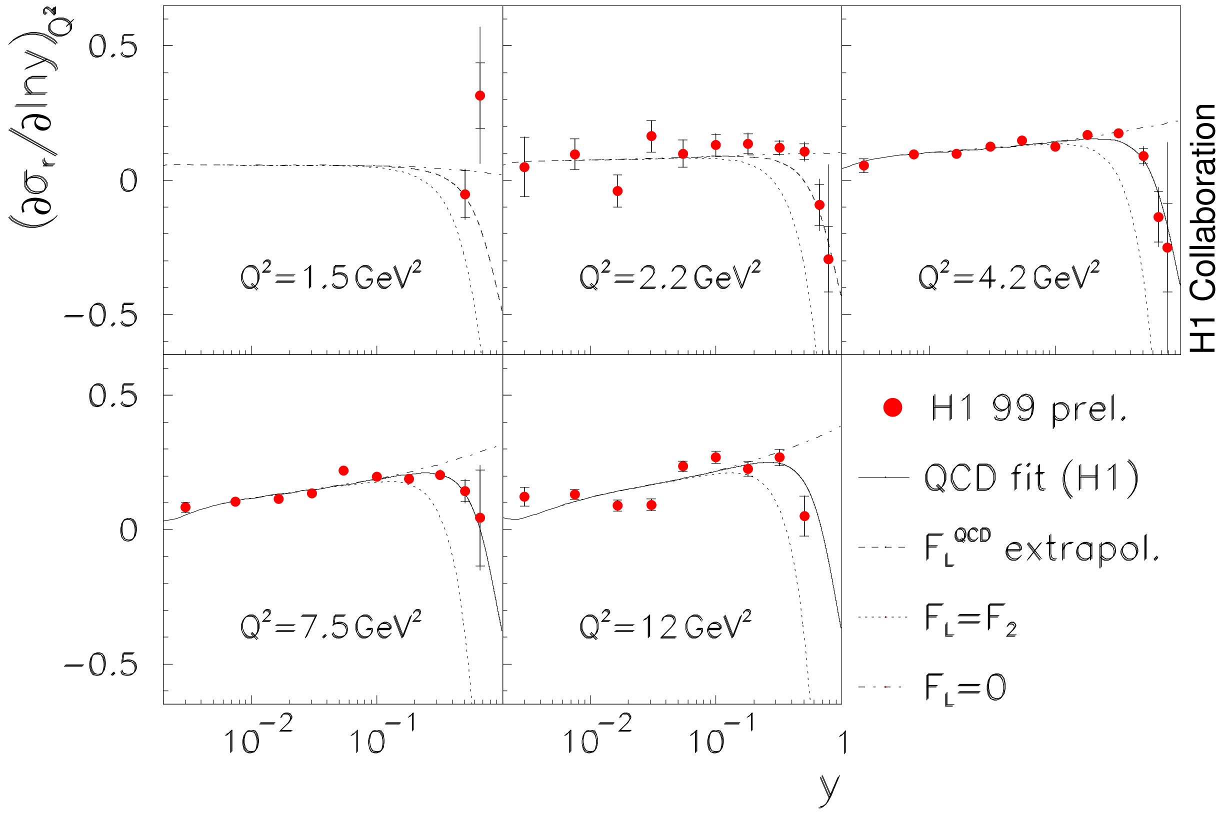

Figure 8: Measurement of the derivative $(\partial\sigma_r/\partial \ln y)_{Q^2}$. The curves represent the QCD fit result to the H1 96/97 data for $y < 0.35$ and $Q^2 \geq 3.5$ GeV^2 calculated with different assumptions on F_L. The inner error bars represent the statistical errors and the total error bars the statistical and systematical errors, added in quadrature.

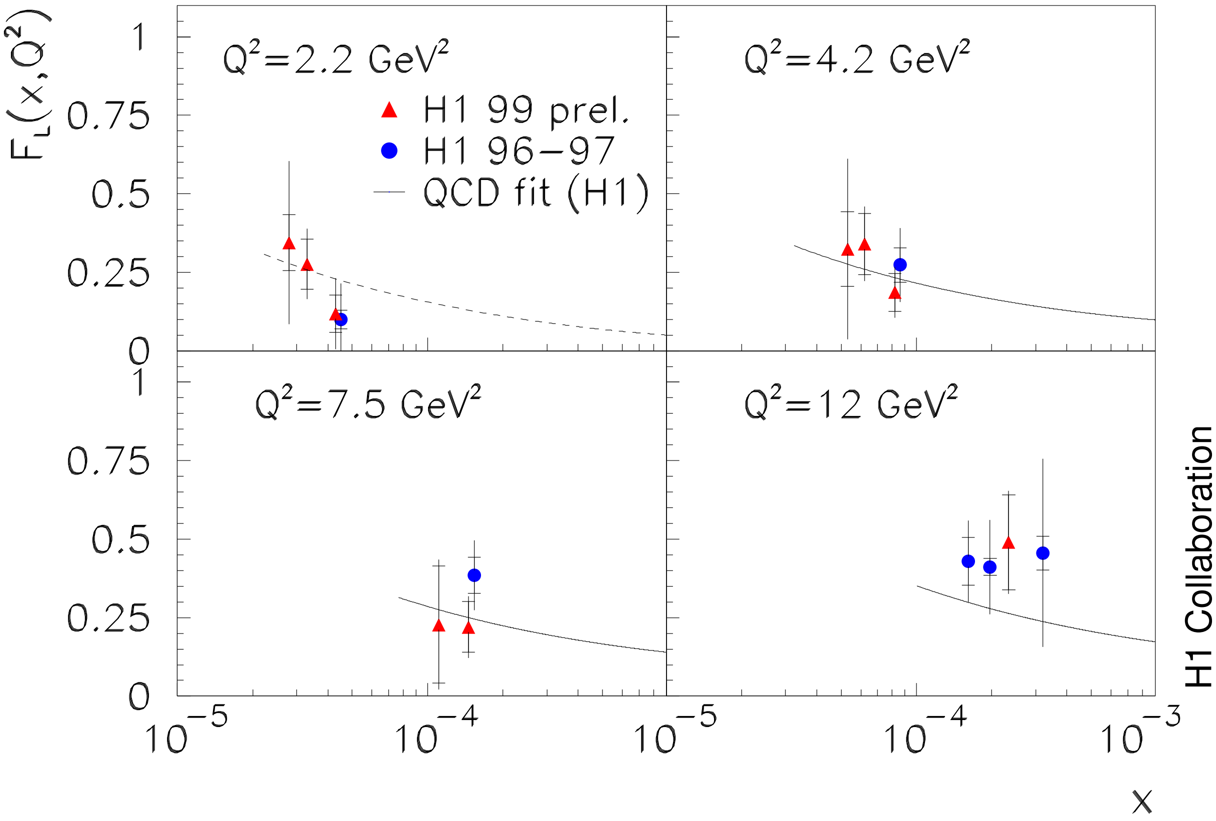

Figure 9: The longitudinal structure function $F_L(x, Q^2)$ determined with the derivative method from the new cross-section data (triangles) compared with the previous result (points).The inner error bars represent the statistical errors and the total error bars the statistical and systematical errors, added in quadrature. The curves represent the QCD fit result to the H1 1996/97 data for $y < 0.35$.

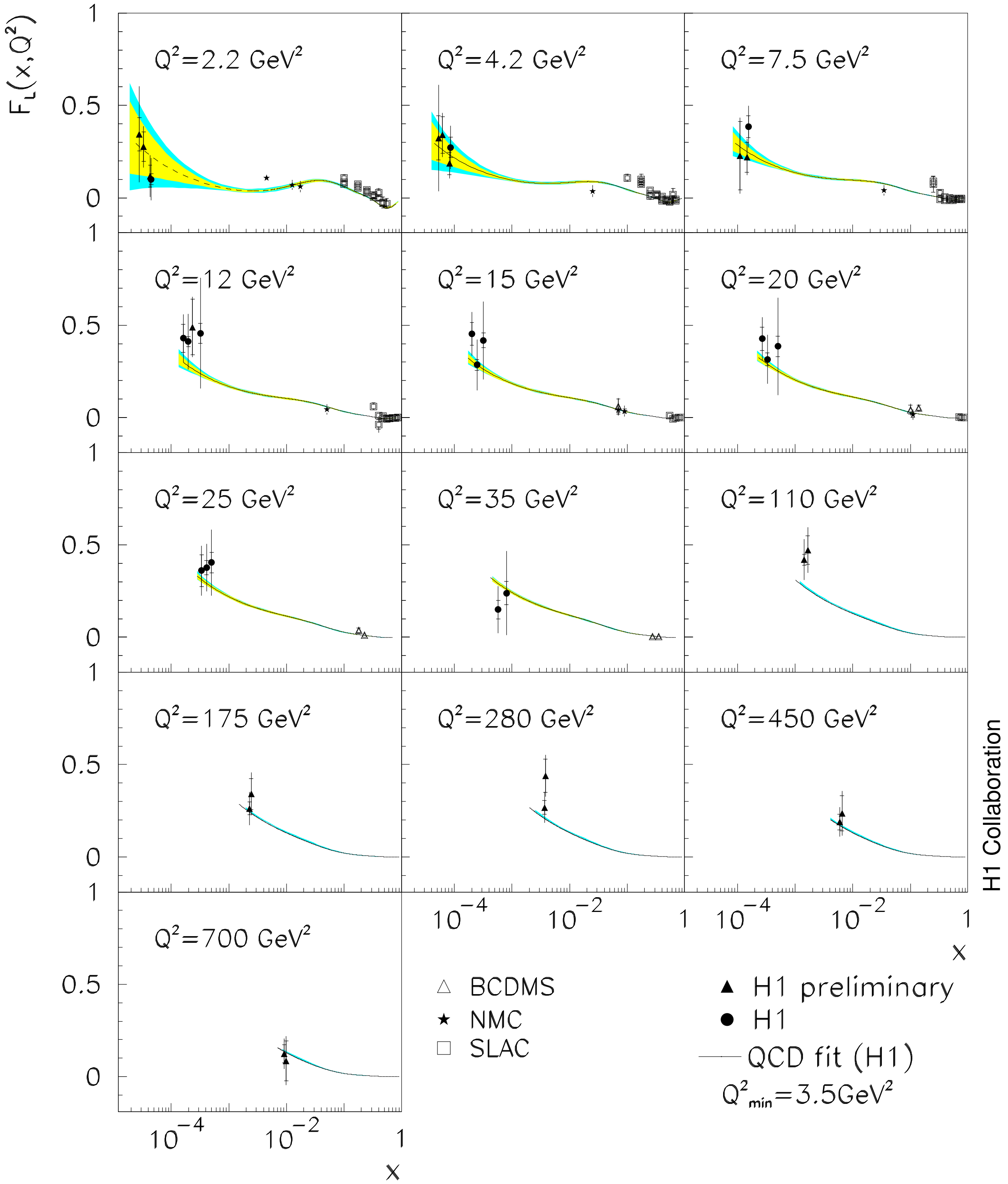

Figure 10: The longitudinal structure function $F_L(x, Q^2)$ as obtained by H1 and by charged lepton-nucleon fixed target experiments. The inner error bars represent the statistical errors and the total error bars the statistical and systematical errors, added in quadrature. The error bands are due to the experimental (inner) and model (outer) uncertainty of the calculation of F_L using the NLO QCD fit to the H1 96/97 data for $y < 0.35$ and $Q^2 \geq 3.5$ GeV^2.